Hydrothermal vents and organic ligands sustained the Precambrian copper budget

E.E. Stüeken[1,2*]

OPEN ACCESS

Abstract

doi: 10.7185/geochemlet.2037

The bioavailability of metals in the early ocean is a key parameter for understanding the evolution and expansion of Earth's biosphere. Theoretical work suggested extremely low Zn and Cu levels in Precambrian seawater, but these predictions are not supported by recent geochemical data. One explanation for this discrepancy is a strong hydrothermal influx of metals and/or stabilisation in solution by organic ligands. Here new models are constructed to test this hypothesis for the solubility of Cu. The results show that hydrothermal vents constituted the major source of Cu to the Archean ocean, but higher ocean temperatures or higher levels of organic matter may have been needed to stabilise dissolved Cu in seawater. From the Proterozoic onwards, rivers contributed most of the marine Cu budget and concentrations were probably close to the modern range, even if the residence time of Cu in seawater was shorter than today. Biological Cu limitation was thus probably lifted in the Proterozoic, but the origin of Cu toxicity for cyanobacteria likely emerged in the Archean. The results provide a new interpretive framework for geochemical records.

Introduction

Transition metals have long been recognised as essential for numerous cellular functions and metabolic pathways. The course of biological evolution from the Archean to the modern may therefore in part have been driven by the bioavailability of these elements in the early ocean. Earlier theoretical work (Saito *et al.*, 2003) suggested extremely low concentrations of Cu and Zn in the Archean and Proterozoic ocean, which triggered several hypotheses about metal-limited biogeochemical cycles. For example, Zn scarcity has been invoked to explain the late rise of eukaryotes, which have a high Zn demand (Dupont *et al.*, 2006), while Cu limitation has been proposed as a mechanism to build up high levels of N_2O in the Proterozoic atmosphere (Buick, 2007). However, recent studies of marine sedimentary rocks do not support Zn- and Cu-depleted oceans in the Precambrian (Scott *et al.*, 2012; Large *et al.*, 2014; Chi Fru *et al.*, 2016; Robbins *et al.*, 2016). To explain this discrepancy, some workers have suggested a stronger hydrothermal metal influx into the ocean (Scott *et al.*, 2012; Robbins *et al.*, 2013). This hypothesis would be consistent with independent evidence that hydrothermal activity was elevated in the early Precambrian compared to today (Viehmann *et al.*, 2015). Indeed, modern hydrothermal vents can disperse metals widely into the open ocean and enhance biological productivity in surface waters (*e.g.*, Fitzsimmons *et al.*, 2014). However, whether this hydrothermal metal flux could have persisted in the Precambrian remains elusive.

To address this knowledge gap, this study explores the role of organic ligands in stabilising hydrothermally sourced Cu in Precambrian seawater. Copper is chosen as a focus, because thermodynamic data are available to model Cu speciation in hydrothermal fluids. Using those data, Sander and Koschinsky (2011) showed that modern hydrothermal vents contribute 5–14 % of the ocean's Cu budget in the form of organic complexes. Here the thermodynamic model is adapted to Precambrian seawater conditions, and subsequently paired with a box model that combines the hydrothermal Cu flux with the riverine flux and the residence of Cu in seawater to derive a global average Cu concentration through time (see Supplementary Information for methods). In brief, the thermodynamic model simulates mixing between a Cu-rich hydrothermal fluid at 300 °C and Cu-depleted seawater at 4 °C up to a ratio of 1:1000 and allows Cu minerals to precipitate. Organic ligands are included in the hydrothermal fluid (L_h^+) and in seawater (L_s^+) with empirically-determined stability constants of 10^{-14} for Cu ligand complexes in both fluids (Sander and Koschinsky, 2011). These constants are assumed to be applicable for the Precambrian models as well. The Cu concentration remaining in solution after precipitation has ceased is then entered into the box model as an input parameter for the hydrothermal Cu source to the ocean. The riverine source is taken from the literature. Both Archean and Proterozoic seawater are modelled as ferruginous (anoxic with 100 μM of free Fe^{2+}) (Holland, 1984), but the Archean is defined by having very low concentrations of SO_4^{2-} (20 μM) and minor amounts of dissolved H_2 (Claire *et al.*, 2006) while the Proterozoic is modelled with 3 mM of SO_4^{2-} in

1. School of Earth & Environmental Sciences, University of St Andrews, Irvine Building, North Street, St Andrews, Fife, KY16 9AL, Scotland, UK
2. Virtual Planetary Laboratory, University of Washington, Seattle, WA-98195, USA
* Corresponding author (email: ees4@st-andrews.ac.uk)

the absence of H$_2$ gas. Sensitivity tests on these parameters are described in the Supplementary Information.

Results

For the modern ocean, the model produced marine Cu concentrations of 2.7–3.4 nM (Fig. 1a), in good agreement with observations of 1–3 nM in the Pacific Ocean (Whitby *et al.*, 2018). Hydrothermal fluids contributed 2–20 % of the total Cu (for L$_h$ of 1–10 μM), similar to the 5–14 % found by Sander and Koschinsky (2011). At the 1000:1 mixing ratio, the concentration of ligand-bound Cu (CuL$_h^+$ and CuL$_s^+$) was of the order of a few nM, while that of free Cu^{2+} was 10^{-13} to 10^{-15} M (Fig. 2), which agrees with measurements from modern seawater (Vraspir and Butler, 2009). The concentration of Cu bound to the seawater ligand (CuL$_s^+$) increased from 0.2 nM to 7 nM at the 1000:1 mixing ratio as the concentration of the hydrothermal ligand L$_h^+$ was raised from 0 to 10 uM (Fig. 2), although L$_s^+$ in seawater stayed constant at 10 nM. This result implies that the hydrothermal ligand prevents some hydrothermally-sourced Cu from precipitating and later passes that Cu on to the seawater ligand as the latter becomes more abundant and thus thermodynamically favourable. Hydrothermal ligands are thus important for

transporting Cu into the ocean. Major precipitates in the modern ocean scenario included chalcocite and ferrite-Cu (Fig. S-2).

In the Archean ocean scenario, even the highest amounts of modern observed ligand concentrations had very little effect on raising total marine Cu concentrations at high mixing ratios with seawater (Cu$_T$; Fig. 1e). Most Cu was lost by the precipitation of Cu sulfides proximal to the vent. The modelled Cu$_T$ concentration was thus always several orders of magnitude below 1 nM. Values closer to the modern range could be obtained if the temperature of seawater was raised to around 50 °C (Fig. 1f), or if the concentration of L$_s^+$ was increased drastically to 1000 μM and the residence time of Cu$_T$ in the ocean was extended to >100,000 yr (Fig. S-7). Increasing L$_h^+$ did not have nearly the same effect as increasing L$_s^+$ (not shown). In any case, the riverine Cu contribution was less than a few percent (Fig. 1e).

In the Proterozoic, modelled Cu$_T$ levels with the maximum modern ligand load (10 μM L$_h^+$ and 10 nM L$_s^+$) were still lower than in the modern, but several orders of magnitude above the Archean. The riverine contribution far outweighed the hydrothermal input (Fig. 1c). Similar to the Archean, high concentrations of L$_s^+$ were needed to establish high marine Cu$_T$ levels similar to the modern. Importantly, lowering the residence time of Cu$_T$ in seawater, as predicted by the expansion of euxinic
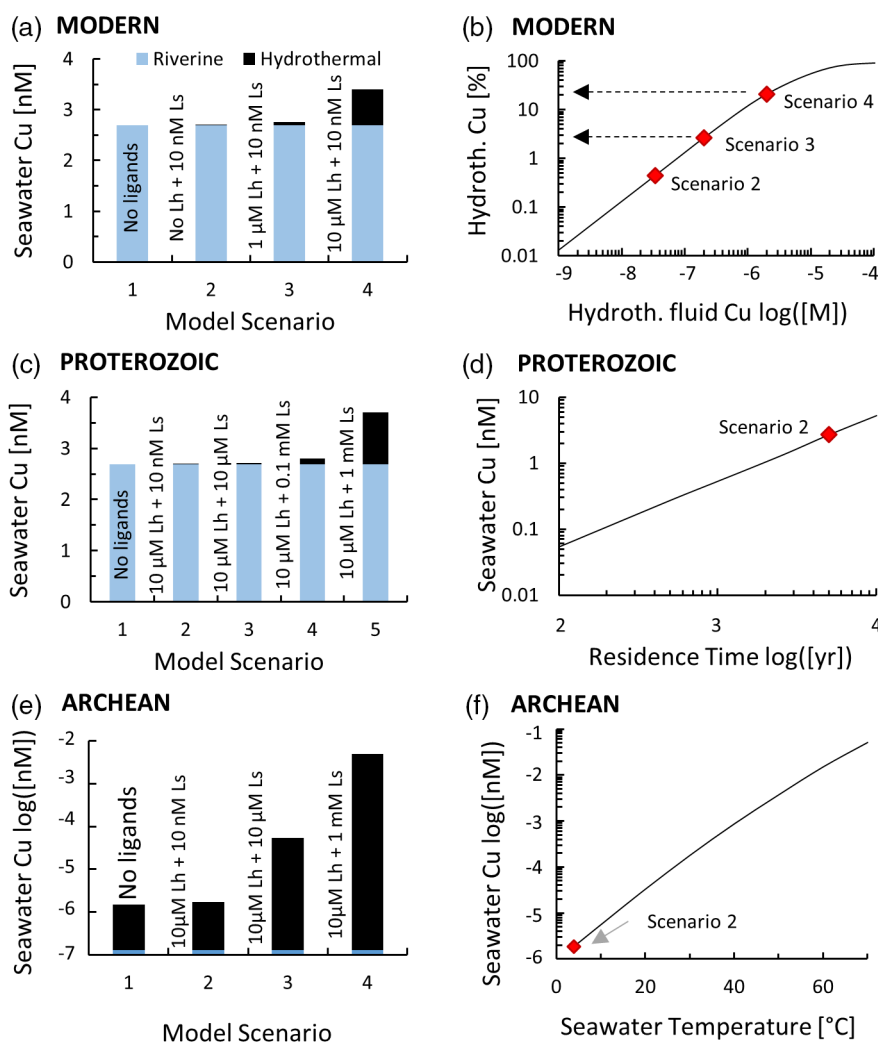
Figure 1 Total Cu concentration in seawater for different model scenarios. **(a)** Modern ocean. **(b)** Fraction of hydrothermal Cu contribution to total marine Cu budget in the modern ocean. Scenarios 3 and 4 are deemed the most realistic according to previous work (Sander and Koschinsky, 2011). **(c)** Proterozoic ocean. **(d)** Effect of the seawater residence time on Cu$_T$ for scenario 2 in the Proterozoic (panel **c**). **(e)** Archean ocean. **(f)** Effect of seawater temperature on Cu$_T$ for scenario 2 in the Archean (panel **e**).
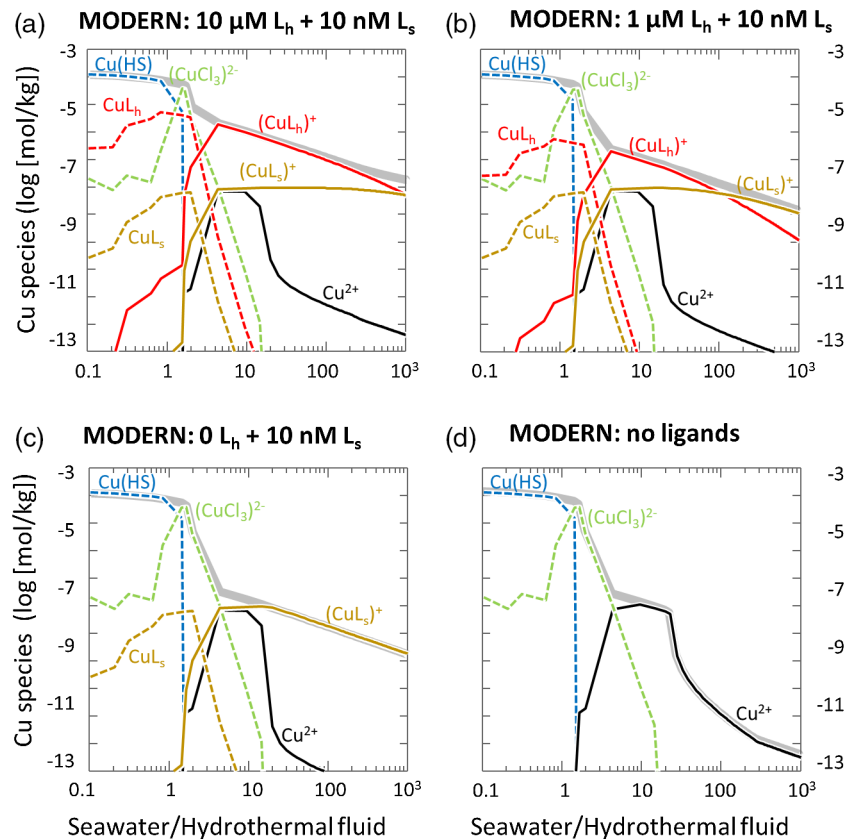
Figure 2 Dissolved copper speciation during mixing between hydrothermal fluid and seawater in the modern ocean under four different model scenarios (see Fig. 1). Note that seawater has an initial Cu_T concentration of zero; the seawater concentration shown in Figure 1 is calculated after combining the hydrothermal mixing model with the ocean box model (Fig. S-1). Solid lines = Cu^{2+} species, dashed lines = Cu^+ species. The x axis shows the mixing ratio of seawater to hydrothermal fluid. Thick solid grey line = Cu_T.

waters along Proterozoic ocean margins (Lyons et al., 2014), did not push Cu_T levels far out of the modern range (Fig. 1d). Sensitivity tests of differing Fe or SO_4^{2-} concentrations within plausible bounds made no significant difference to the overall conclusions (Tables S-2, S-3).

Discussion

In the Archean, only high seawater temperatures (Fig. 1f) or unusually high concentrations of organic ligands in seawater paired with a much longer seawater residence time of Cu_T may have been able to push Cu_T concentrations closer to modern values. It is conceivable that the amount of suspended organic matter in seawater was indeed higher in the Precambrian, prior to the rise of filter feeding metazoans and complex algae (Lenton et al., 2014). For example, a microbially-dominated anoxic lake in Antarctica, which lacks significant input of eukaryotic biomass, reaches DOC levels up to 2000 μM (McKnight et al., 1991). If a high proportion of the organic matter was Cu-binding, it may thus have increased the residence time and concentration of Cu_T in seawater, which may explain the nearly constant Cu levels in sedimentary rocks through time (Large et al., 2014; Chi Fru et al., 2016). Alternatively, the unexpectedly high Archean Cu enrichments in rocks may reflect higher seawater temperatures (Tartèse et al., 2017), which would have raised the solubility of Cu sulfide minerals.

Throughout the Archean, hydrothermal vents were the major source of Cu to the ocean, because the riverine flux was low in the absence of oxidative weathering (Hao et al., 2017). Interestingly, previous workers have pointed out that several

prebiotic reactions may have occurred in hydrothermal settings because of the abundance of catalytic metals (Martin et al., 2008). The results from this study suggest that Cu_T concentrations were closest to modern values proximal to hydrothermal vents where the mixing ratio of seawater to vent fluid was lower (Fig. 3). Hence the model supports the view that the origin of metalloenzymes occurred proximal to hydrothermal environments. At the same time, the dispersal of ligand-bound Cu into the global ocean from hydrothermal point sources may be consistent with the idea that prebiotic hydrothermal products may have undergone further modification and evolution in other environmental niches (Stüeken et al., 2013).

With the onset of oxidative sulfide weathering in the Proterozoic (the most probable Cu source to rivers), Cu_T levels were probably within 1–2 orders of magnitude of modern concentrations (Fig. 1d). Throughout the Proterozoic (Fig. 3c,d) and the modern (Fig. 2), and possibly earlier (Fig. 3b), Cu_T was largely organic-bound, which would explain the difference between these new results and earlier predictions (Saito et al., 2003). Unlike in the Archean, rivers largely controlled the marine Cu_T budget of the Proterozoic, but it is important to note that riverine Cu would also have needed to be ligand-bound to be stable in the Proterozoic ocean, as suggested by the seawater end member composition of the thermodynamic model (Fig. 3) and consistent with observations from modern rivers where Cu is overwhelmingly organic-bound (Hoffmann et al., 2007). Ligand-bound Cu can be bioavailable (Zhao et al., 2016), making it unlikely that Cu was bio-limiting in the Proterozoic and that Cu limitation caused large scale production of N_2O gas (Buick, 2007). One the other hand, Cu toxicity to cyanobacteria may
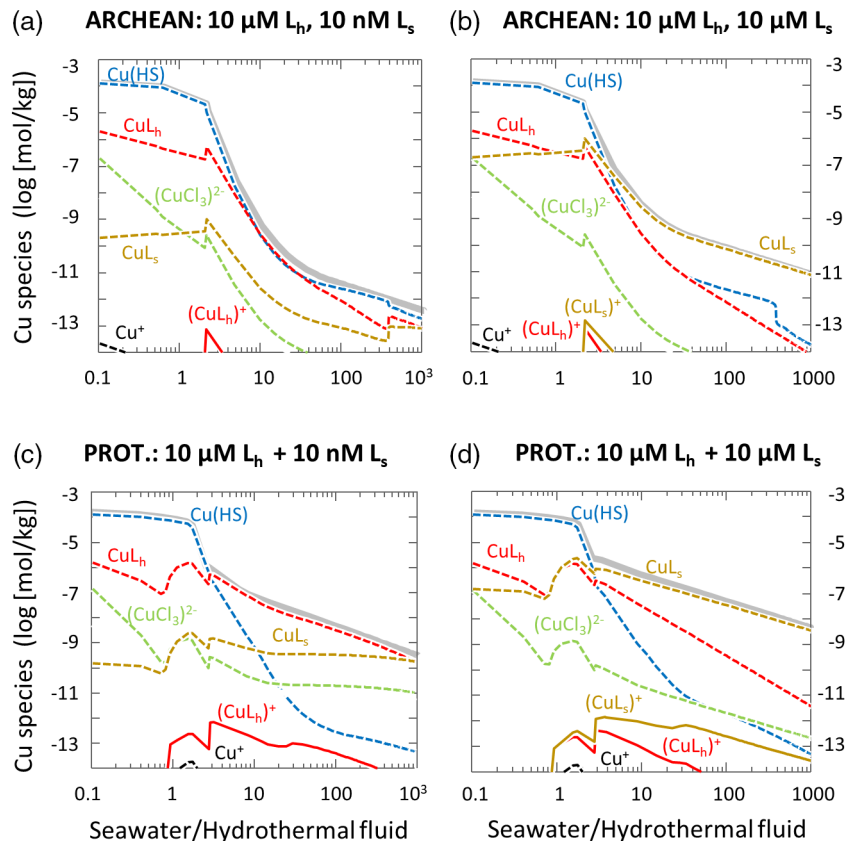
Figure 3 Dissolved copper speciation in the Archean (a, b) and Proterozoic (c, d) during mixing between hydrothermal fluid and seawater, showing two different model scenarios for each time bin. As for Figure 2, seawater Cu_T is set to zero in these simulations and then calculated with the ocean box model in a separate step (Fig. S-1). Colour code and symbols as in Figure 2. In the absence of ligands, aqueous Cu(HS) is the dominant species in both the Archean and Proterozoic ocean (not plotted). Thick solid grey line = Cu_T.
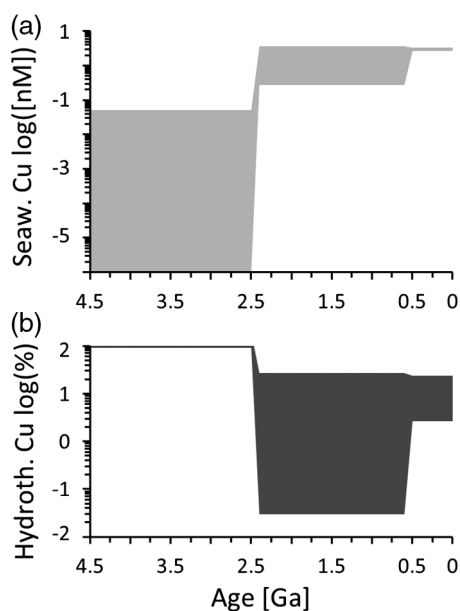
Figure 4 Compilation of (a) the total marine Cu concentration and (b) the hydrothermal contribution to the marine Cu budget through time. For the Archean, the lower bound is scenario 2 in Figure 1e; the upper bound corresponds to scenario 4 in Figure 1e with a 10-fold longer residence time (Fig. S-7). For the Proterozoic, the lower bound is scenario 2 in Figure 1c with a 10-fold shorter residence time (Fig. 1d) while the upper bound corresponds to scenario 5 in Figure 1c with a modern residence time.

have arisen earlier than previously thought. It has been shown that free Cu^{2+} concentrations around 10^{-11} M can negatively impact both CO_2 and N_2 fixation (Rueter and Petersen, 1987). This Cu sensitivity may be an artifact of a relatively Cu-free setting during the origin of cyanobacteria. If so, then the model of this study would support the idea that cyanobacteria originated in the Archean (Lyons et al., 2014), prior to the expansion of the marine Cu_T budget.

Conclusion

Our understanding of Precambrian ocean chemistry has evolved since the original study by Saito et al. (2003) that predicted severe Cu limitation in the Archean and Proterozoic due to rapid scavenging of Cu by free H_2S. It is now evident that such H_2S-rich conditions were spatially limited in the early oceans (Lyons et al., 2014), warranting a new model of Cu_T solubility. The results presented here support the inference that Archean Cu_T levels were probably lower than today (Fig. 4a), unless seawater was warmer or the abundance of organic ligands was markedly higher. Near modern levels of Cu_T were likely reached in the Proterozoic with the onset of oxidative weathering, despite a potentially shorter residence time in the ocean. In the Archean, hydrothermal vents constituted the major source of Cu (Fig. 4b), which provides additional credence to the idea that key prebiotic processes involving the origin of metalloenzymes occurred in hydrothermal settings. From the Proterozoic onwards, and perhaps earlier, the vast majority of Cu_T in seawater has been stabilised by organic ligands, which thus probably lifted Cu limitations for the evolving biosphere. While the model presented in this study

focused on Cu only, it is predicted that similar mechanisms would apply for Zn and perhaps other base metals.

Acknowledgements

Additional Information

References

Buick, R. (2007) Did the Proterozoic 'Canfield Ocean' cause a laughing gas greenhouse? *Geobiology* 5, 97–100.

Chi Fru, E., Rodríguez, N.P., Partin, C.A., Lalonde, S.V., Andersson, P., Weiss, D.J., El Albani, A., Rodushkin, I., Konhauser, K.O. (2016) Cu isotopes in marine black shales record the Great Oxidation Event. *Proceedings of the National Academy of Sciences* 113, 4941–4946.

Claire, M.W., Catling, D.C., Zahnle, K.J. (2006) Biogeochemical modelling of the rise in atmospheric oxygen. *Geobiology* 4, 239–269.

Dupont, C.L., Yang, S., Palenik, B., Bourne, P.E. (2006) Modern proteomes contain putative imprints of ancient shifts in trace metal geochemistry. *Proceedings of the National Academy of Sciences* 103, 17822–17827.

Fitzsimmons, J.N., Boyle, E.A., Jenkins, W.J. (2014) Distal transport of dissolved hydrothermal iron in the deep South Pacific Ocean. *Proceedings of the National Academy of Sciences* 111, 16654–16661.

Hao, J., Sverjensky, D.A., Hazen, R.M. (2017) Mobility of nutrients and trace metals during weathering in the late Archean. *Earth and Planetary Science Letters* 471, 148–159.

Hoffmann, S.R., Shafer, M.M., Armstrong, D.E. (2007) Strong colloidal and dissolved organic ligands binding copper and zinc in rivers. *Environmental Science & Technology* 41, 6996–7002.

Holland, H.D. (1984) *The chemical evolution of the atmosphere and oceans*. Princeton University Press, Princeton, NJ.

Large, R.R., Halpin, J.A., Danyushevsky, L.V., Maslennikov, V.V., Bull, S.W., Long, J.A., Gregory, D.D., Lounejeva, E., Lyons, T.W., Sack, P.J., McGoldrick, J.J., Calver, C.R. (2014) Trace element content of sedimentary pyrite as a new proxy for deep-time ocean-atmosphere evolution. *Earth and Planetary Science Letters* 389, 209–220.

Lenton, T.M., Boyle, R.A., Poulton, S.W., Shields-Zhou, G.A., Butterfield, N.J. (2014) Co-evolution of eukaryotes and ocean oxygenation in the Neoproterozoic era. *Nature Geoscience* 7, 257–265.

Lyons, T.W., Reinhard, C.T., Planavsky, N.J. (2014) The rise of oxygen in Earth's early ocean and atmosphere. *Nature* 506, 307–315.

Martin, W., Baross, J., Kelley, D., Russell, M.J. (2008) Hydrothermal vents and the origin of life. *Nature Reviews Microbiology* 6, 805–814.

McKnight, D.M., Aiken, G.R., Smith, R.L. (1991) Aquatic fulvic acids in microbially based ecosystems: results from two desert lakes in Antarctica. *Limnology and Oceanography* 36, 998–1006.

Robbins, L.J., Lalonde, S.V., Saito, M.A., Planavsky, N.J., Miloszewska, A.M., Pecoits, E., Scott, C., Dupont, C.L., Kappler, A., Konhauser, K. (2013) Authigenic iron oxide proxies for marine zinc over geological time and implications for eukaryotic metallome evolution. *Geobiology* 11, 295–306.

Robbins, L.J., Lalonde, S.V., Planavsky, N.J., Partin, C.A., Reinhard, C.T., Kendall, B., Scott, C., Hardisty, D.S., Gill, B.C., Alessi, D.S., Dupont, C.L. (2016) Trace elements at the intersection of marine biological and geochemical evolution. *Earth-Science Reviews* 163, 323–348.

Rueter, J.G., Petersen, R.R. (1987) Micronutrient effects on cyanobacterial growth and physiology. *New Zealand Journal of Marine and Freshwater Research* 21, 435–445.

Saito, M.A., Sigman, D.M., Morel, F.M.M. (2003) The bioinorganic chemistry of the ancient ocean: the co-evolution of cyanobacterial metal requirements and biogeochemical cycles at the Archean-Proterozoic boundary? *Inorganica Chimica Acta* 356, 308–318.

Sander, S.G., Koschinsky, A. (2011) Metal flux from hydrothermal vents increased by organic complexation. *Nature Geoscience* 4, 145–150.

Scott, C., Planavsky, N.J., Dupont, C.L., Kendall, B., Gill, B.C., Robbins, L.J., Husband, K.F., Arnold, G.L., Wing, B., Poulton, S.W., Bekker, A., Anbar, A., Konhauser, K., Lyons, T.W. (2012) Bioavailability of zinc in marine systems through time. *Nature Geoscience* 6, 125–128.

Stüeken, E.E., Anderson, R.E., Bowman, J.S., Brazelton, W.J., Colangelo-Lillis, J., Goldman, A.D., Som, S.M., Baross, J.A. (2013) Did life originate from a global chemical reactor? *Geobiology* 11, 101–126.

Tartèse, R., Chaussidon, M., Gurenko, A., Delarue, F., Robert, F. (2017) Warm Archean oceans reconstructed from oxygen isotope composition of early-life remnants. *Geochemical Perspectives Letters* 3, 55–65.

Viehmann, S., Bau, M., Hoffmann, J.E., Münker, C. (2015) Geochemistry of the Krivoy Rog Banded Iron Formation, Ukraine, and the impact of peak episodes of increased global magmatic activity on the trace element composition of Precambrian seawater. *Precambrian Research* 270, 165–180.

Vraspir, J.M., Butler, A. (2009) Chemistry of marine ligands and siderophores. *Annual Review of Marine Science* 1, 43–63.

Whitby, H., Posacka, A.M., Maldonado, M.T., van den Berg, C.M. (2018) Copper-binding ligands in the NE Pacific. *Marine Chemistry* 204, 36–48.

Zhao, C.-M., Campbell, P.G., Wilkinson, K.J. (2016) When are metal complexes bioavailable? *Environmental Chemistry* 13, 425–433.

Hydrothermal vents and organic ligands sustained the Precambrian copper budget

E.E. Stüeken

Supplementary Information

The Supplementary Information includes:

Thermodynamic Model

The thermodynamic model of mixing between hydrothermal fluid and seawater was set up in Geochemist's Workbench® (GWB, version 12.0.4), following the approach of Sander and Koschinsky (2011). The composition of the modern Rainbow hydrothermal vent field at the Mid-Atlantic Ridge was used to represent the hydrothermal endmember (Table S-1). Modern seawater (28.2 mM SO_4^{2-}, 0.7 nM Fe^{3+}) was initially equilibrated with 0.21 bar O_2 gas, resulting in 349 µM $O_{2(aq)}$. This composition was then used as a reactant in the model, *i.e.* disconnected from the atmospheric O_2 reservoir. The initial total dissolved copper (Cu_T) concentration of seawater was set to 0 in all cases. For the Proterozoic, seawater was equilibrated with 0.0021 bar O_2 (1 % present levels) (Lyons *et al.*, 2014), giving $3.5 \cdot 10^{-6}$ M $O_{2(aq)}$. This composition was then equilibrated with Fe^{2+} and SO_4^{2-} set to 100 µM (Holland, 1984) and 3 mM (Luo *et al.*, 2014), respectively. This two-step approach mimics mixing of oxygen-charged surface waters with anoxic deep waters. The final composition was anoxic (10^{-51} M $O_{2(aq)}$) and dominated by Fe^{2+} (ferruginous), consistent with observations (Planavsky *et al.*, 2011). For the Archean, Fe^{2+} was kept at 100 µM while SO_4^{2-} was set to 20 µM (Jamieson *et al.*, 2013; Crowe *et al.*, 2014). Instead of O_2, Archean seawater was equilibrated with 10^{-5} bar H_2 gas (giving $5.6 \cdot 10^{-9}$ M $H_{2(aq)}$) as suggested for the Archean atmosphere (Claire *et al.*, 2006). The final composition was thus also anoxic and ferruginous, but more reducing than in the Proterozoic. It is important to note in this context that the term ferruginous can have two different meanings: The Archean state where sulfur is stable as H_2S (though added here as SO_4^{2-}), but Fe^{2+} is relatively more abundant than H_2S, and the Proterozoic state where sulfur is present as SO_4^{2-}

while iron is stable as Fe^{2+}. The latter would have a relatively higher redox potential. To explore the sensitivity of the model, Fe^{2+} concentrations up to 1 mM were tested for the Proterozoic and Archean (Tosca *et al.*, 2016) but not found to have any significant effect on the final results (Tables S-2 and S-3). For the Proterozoic model, changing SO_4^{2-} concentrations in the range of 3-10 mM also had negligible effects (< few % difference), but decreasing SO_4^{2-} to 2 mM or less generated results more akin to the Archean. For the Archean model, lowering SO_4^{2-} to 2 µM (Crowe *et al.*, 2014) made no discernible difference while increasing it to 0.2-2 mM increased the final total Cu concentration in the hydrothermal fluid by about one order of magnitude, but this does not impact the overall conclusion of very low Archean Cu_T levels.

The hydrothermal fluid (T = 300 °C) was mixed with seawater (T = 4 °C) in proportions from 0.1 to 1000 and the fluid chemistry was monitored. To model the speciation of Cu in the presence of organic ligands, the *thermo* database in GWB was modified, following Sander and Koschinsky (2011). A hydrothermal ligand (L_h) and a seawater ligand (L_s) for Cu were added with their known dissociation constants. Also $Cu(HS)^+_{(aq)}$ and $Cu(HS)_{(aq)}$ were added as aqueous complexes (Al-Farawati and van den Berg, 1999). The initial concentration of the two ligands, based on modern observations (Sander and Koschinsky, 2011) was set to 10 nM for L_s in seawater and 0 µM, 1 µM or 10 µM for L_h in the hydrothermal fluid. Other concentrations were explored as described below. Precipitation was allowed for the following minerals: pyrite, pyrrhotite, sphalerite, galena, amorphous $Fe(OH)_3$ and $Fe(OH)_2$, birnessite, cuprite, covellite, copper, chalcopyrite, chalcocite, ferrite-Cu, malachite, azurite, barite, anhydrite, nontronite, talc and amorphous SiO_2. All major ion concentrations in the seawater endmember prior to mixing with the hydrothermal fluid were kept constant through time. The pH of the seawater endmember was varied from 6.5 in the Archean to 7.5 in the Proterozoic and 8.1 in the Phanerozoic (Halevy and Bachan, 2017; Isson and Planavsky, 2018; Krissansen-Totton *et al.*, 2018).

The REACT module of Geochemis's Workbench® was used for the thermodynamic model. The hydrothermal fluid was entered as a Basis with a total amount of 1 kg. Seawater, also 1 kg, was entered as a Reactant, and 'reactant times' was set to 1000, which allows progressive mixing of the two fluids up to a ratio of 1:1000. Under Config → Iteration, *precipitation* was turned on; all other parameters were left at their default values. Under Config → Stepping, *delxi* (the maximum allowed step in the reaction) was set to 0.0001, which allows monitoring fluid changes at lower mixing ratios. Under 'special configurations', *flow-through* and *dump* were ticked. The *dump* function forces the programme to precipitate minerals that are saturated prior to the reaction. This is a realistic scenario, because it removes saturated minerals that would naturally precipitate from a hydrothermal fluid prior to mixing with seawater. The *flow-through* function prohibits precipitated minerals to re-dissolve, which mimics settling of minerals to the seafloor, as observed in natural systems.

Box Model

Sander and Koschinsky (2011) used the end-product at a mixing ratio of 1000:1 to evaluate the imprint of hydrothermal venting on the marine Cu_T budget. However, this mixing ratio is not easily justified. In this study, the thermodynamic model was thus followed by a box model of Cu_T in the ocean, run in Stella® Professional (version 1.0.1). The box model (Fig. S-1) included a riverine (F_{river}) and a hydrothermal input flux ($F_{hydrothermal}$) of Cu in units of mol/yr. For the hydrothermal flux, the global average hydrothermal water flux of today (10^{14} L/yr) (Reinhard *et al.*, 2013) was multiplied by the total Cu concentration in mol/L obtained from the thermodynamic model at that point where precipitation had ceased. This point was chosen because it represents the moment when the mixed fluid disperses freely into the ocean without further precipitation near the vent environment. The river flux was calculated as the product of the global average river water flux ($3.74 \cdot 10^{16}$ L yr^{-1}) (Emerson and Hedges, 2008) and the average Cu concentration in rivers today ($2 \cdot 10^{-8}$ M) (Little *et al.*, 2013). For the Proterozoic, the river water flux and concentration were kept at the modern value, because oxidative weathering is thought to have started around 2.7-2.5 Ga (Stüeken *et al.*, 2012). For the Archean, the river water flux was kept constant but the riverine Cu concentration was set to 10^{-15} M (Hao *et al.*, 2017). It is likely that past river fluxes were lower when continents were smaller (Holland, 1984; Raiswell, 2006) while hydrothermal water fluxes may have been higher when the Earth was hotter.
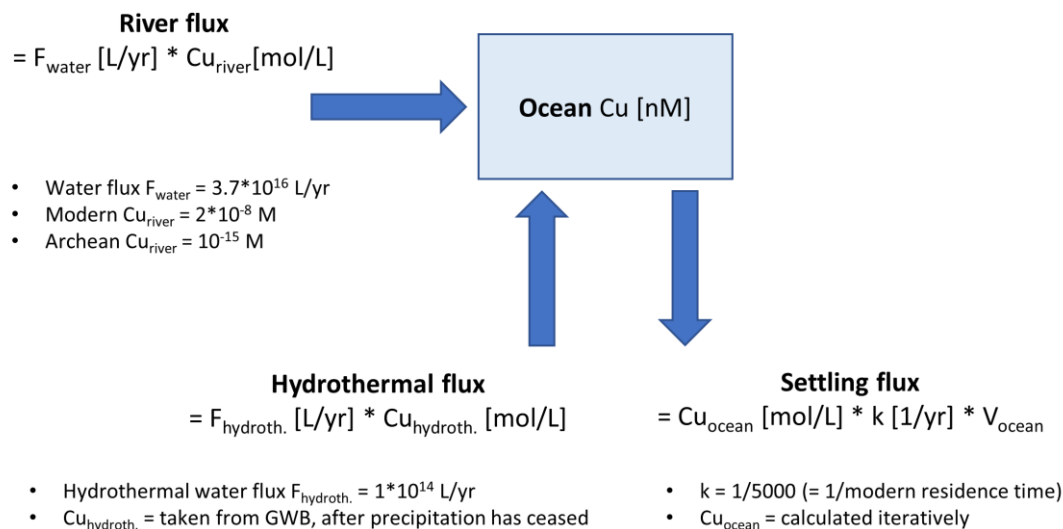
The uncertainty bounds on these parameters are unknown and therefore not explored in detail in this model. Using a lower river water flux of $3 \cdot 10^{15}$ L yr^{-1} (Holland, 1984; Raiswell, 2006) would lower the total Cu concentration of the Proterozoic by roughly one order of magnitude (Fig. S-6), but the broad trends in Cu$_T$ from the Archean to the modern and the relative contribution of hydrothermal Cu sources are not affected. Furthermore, the lower river flux was estimated for the Archean; in the Proterozoic when continental land mass had approached Phanerozoic levels, it is likely that the river flux was closer to the modern value. The Archean total Cu concentration does not change if the river water flux is reduced (not shown), because hydrothermal fluids by far outweigh the marine Cu budget. The sink of Cu from the ocean (F_{sink}) was modelled as a first-order reaction ($F_{sink} = V_{ocean} \cdot [Cu]_{ocean} \cdot k$) with a rate constant ($k$) equal to 1/5000 yr^{-1}, where 5000 yr is the residence time of Cu in the modern ocean (Hao *et al.*, 2017). V_{ocean} is the volume of the ocean, set equal to the modern value, and *[Cu]$_{ocean}$* is the marine Cu$_T$ concentration in mol/L. This residence time, *i.e.* the rate constant for Cu$_T$ removal from the ocean, was varied as described below to explore the effects of Proterozoic euxinia (Lyons *et al.*, 2014). To test the relative contributions of hydrothermal and riverine Cu to the total ocean budget, the box model was run with each source flux turned on separately. The box model was run until an equilibrium value for *[Cu]$_{ocean}$* was reached, which was taken as the final result.

Supplementary Figures

River flux
$= F_{water}\ [L/yr] * Cu_{river}[mol/L]$

Ocean Cu [nM]

- Water flux $F_{water} = 3.7*10^{16}$ L/yr
- Modern $Cu_{river} = 2*10^{-8}$ M
- Archean $Cu_{river} = 10^{-15}$ M

Hydrothermal flux
$= F_{hydroth.}\ [L/yr] * Cu_{hydroth.}\ [mol/L]$

- Hydrothermal water flux $F_{hydroth.} = 1*10^{14}$ L/yr
- $Cu_{hydroth.}$ = taken from GWB, after precipitation has ceased

Settling flux
$= Cu_{ocean}\ [mol/L] * k\ [1/yr] * V_{ocean}$

- k = 1/5000 (= 1/modern residence time)
- Cu_{ocean} = calculated iteratively

Figure S-1 Schematic of the box model run in Stella®. F_{water} = river water flux; Cu_{river} = concentration of Cu in river water; $F_{hydroth.}$ = hydrothermal water flux; $Cu_{hydroth.}$ = hydrothermal Cu concentration, taken from the thermodynamic model after precipitation has ceased; Cu_{ocean} = Cu_T concentration in seawater, i.e. target parameter of the box model; k = rate constant for Cu settling out of the ocean; V_{ocean} = total ocean volume in litres. The system was solved by integration with the Euler method.
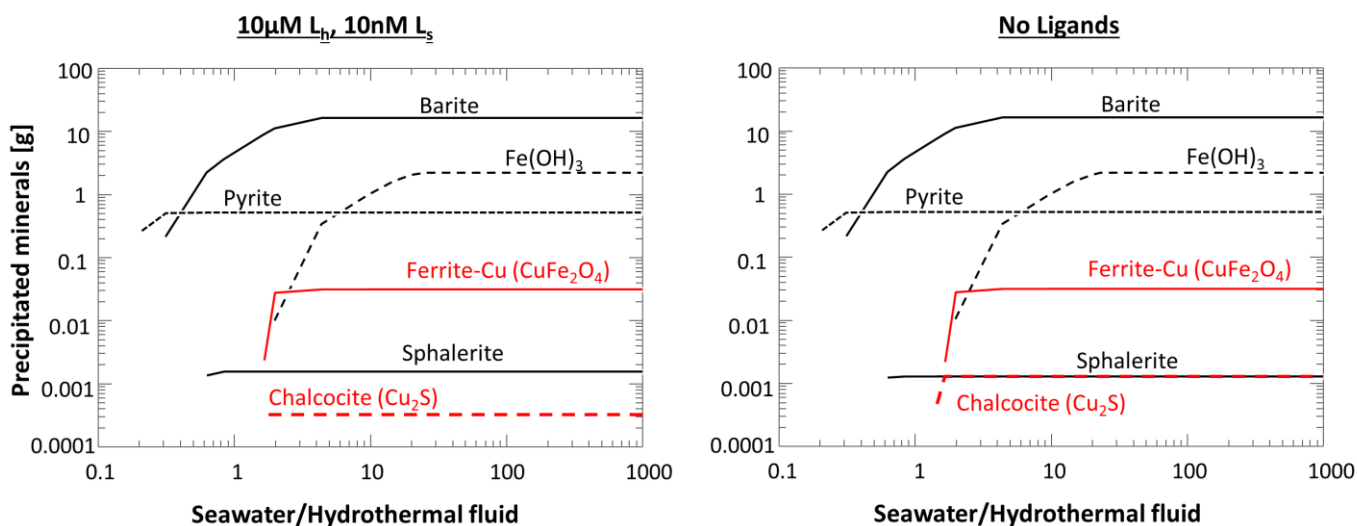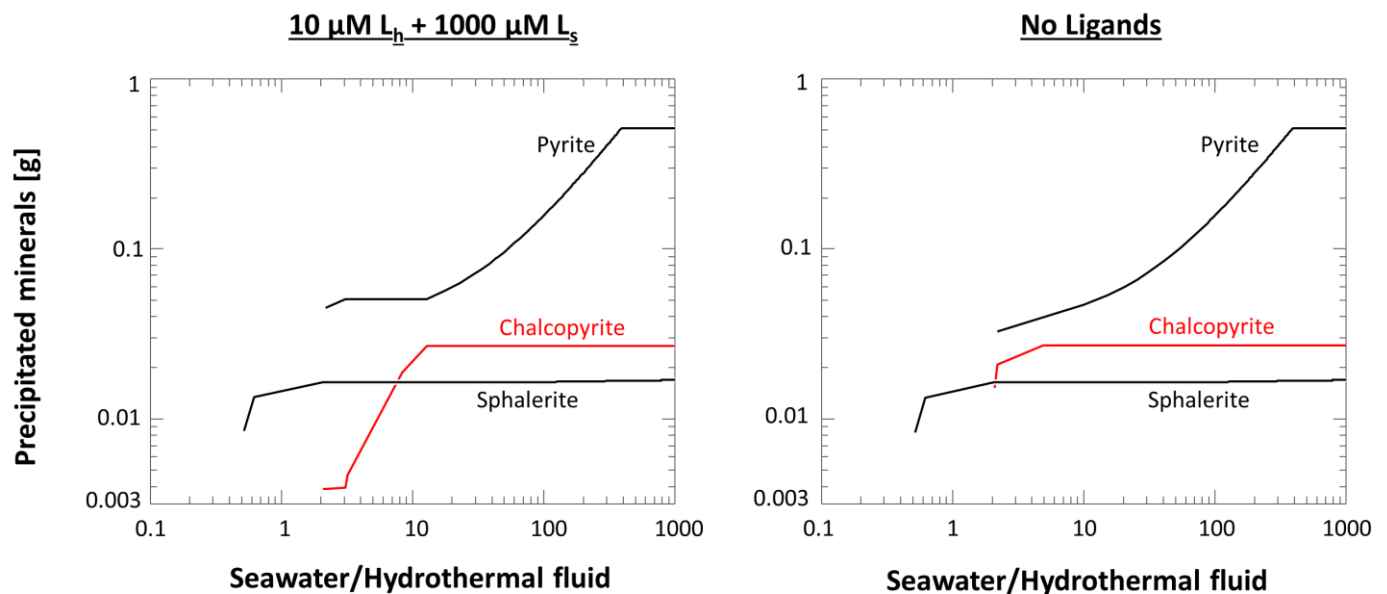

Figure S-2 Mineral precipitation in the modern ocean during mixing between 1 kg hydrothermal fluid and up to 1000 kg seawater. Copper-bearing minerals are marked in red. Note that less chalcocite is precipitated in the presence of ligands.
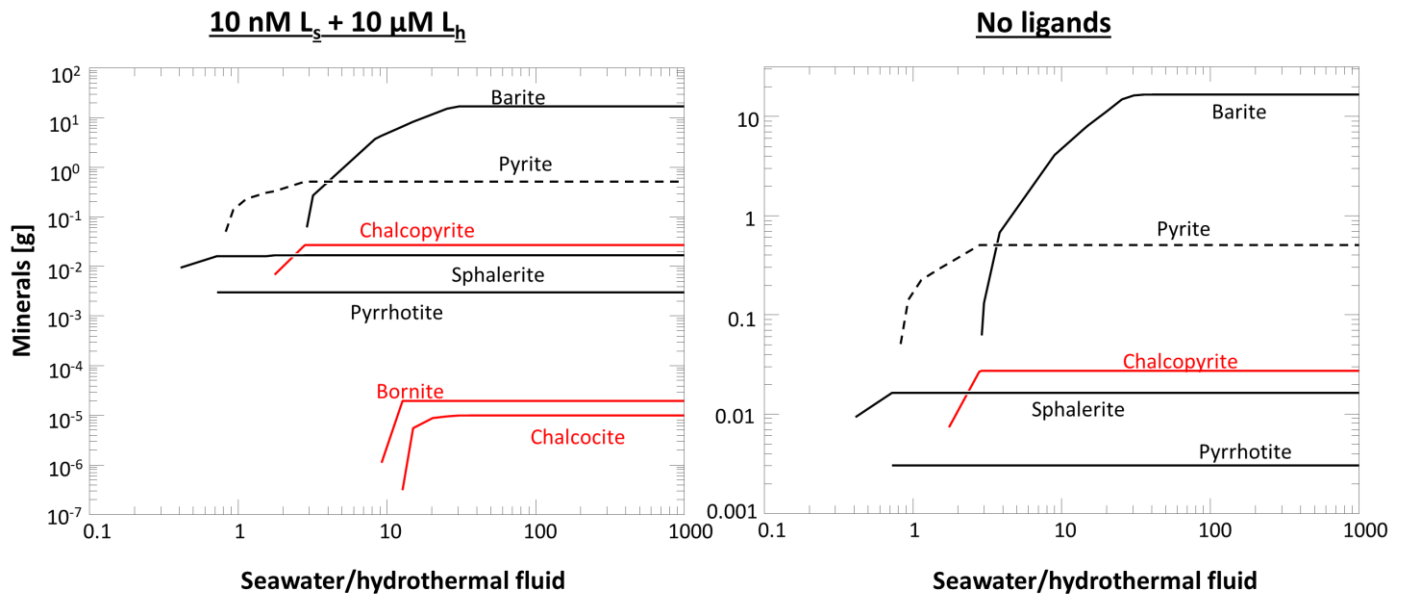
Figure S-3 Mineral precipitation in the Proterozoic ocean during mixing between 1 kg hydrothermal fluid and up to 1000 kg seawater. Copper-bearing minerals are marked in red. Less chalcopyrite is precipitated in the presence of ligands, but the difference is not visible at this scale. Note change in mineral speciation towards more Fe-depleted Cu phases (chalcocite and bornite) in the presence of ligands, which results from Cu-release from the hydrothermal ligand later during the mixing process.


Figure S-4 Mineral precipitation in the Archean ocean during mixing between 1 kg hydrothermal fluid and up to 1000 kg seawater. Copper-bearing minerals are marked in red. Note that chalcopyrite precipitates later in the presence of ligands and overall less of it is produced.
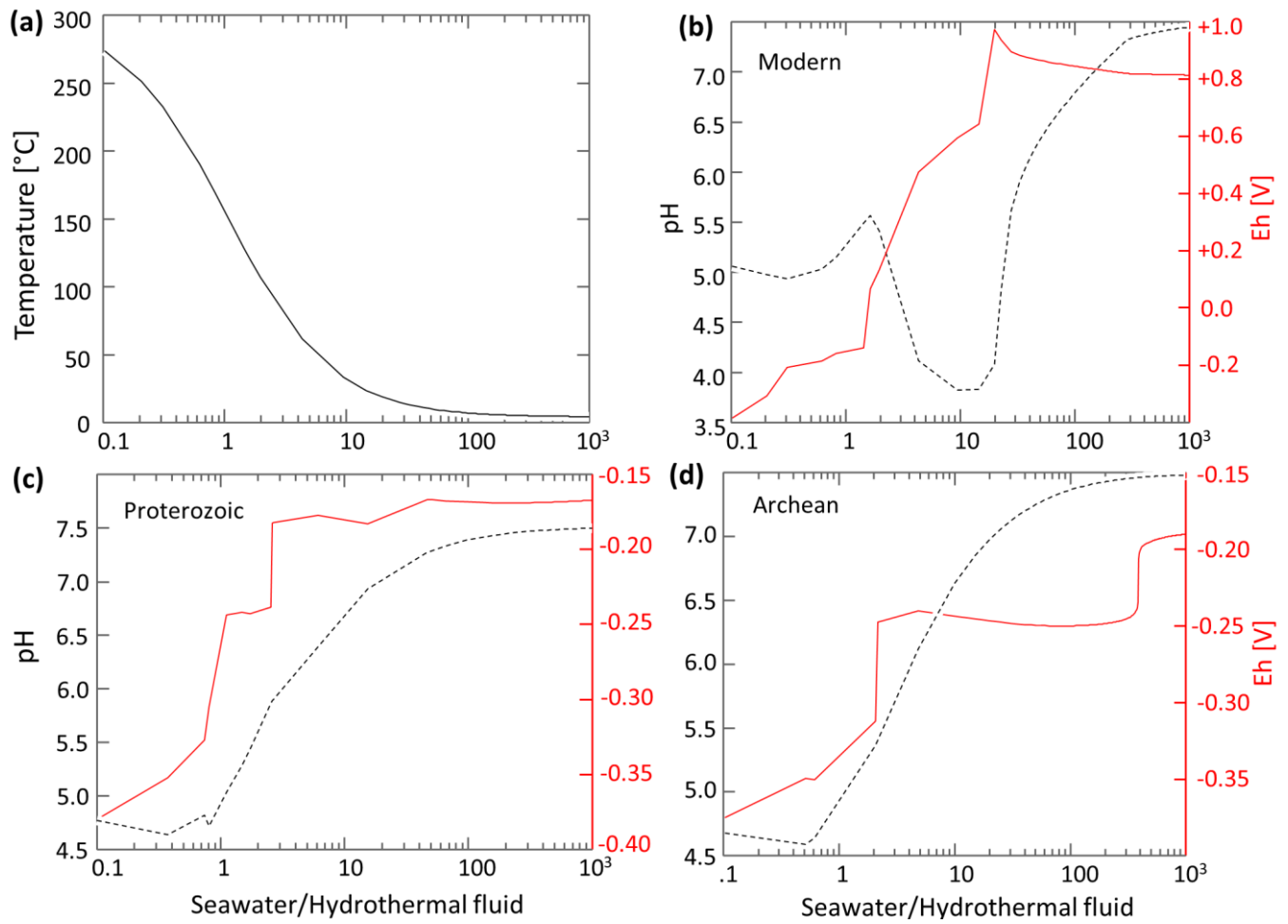
Figure S-5 Change in fluid temperature **(a)**, as well as pH and Eh for the modern **(b)**, Proterozoic **(c)** and Archean **(d)** scenario. The temperature change in panel **(a)** applies to all three time periods.
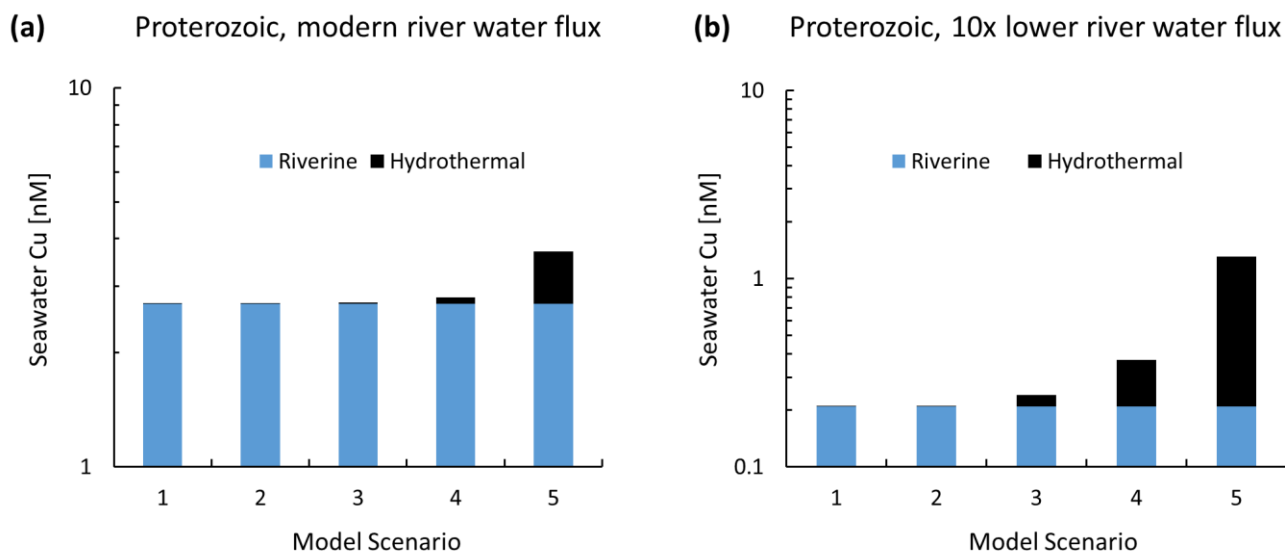
Figure S-6 Comparing the effect of different total river water fluxes on the marine Cu budget in the Proterozoic ocean. **(a)** Using the modern river water flux of $3.74 \cdot 10^{16}$ L yr^{-1} (same as Figure 1c in the main text). **(b)** Using a lower river water flux of $3 \cdot 10^{15}$ L yr^{-1}. The total marine Cu concentration in **(b)** is lower by roughly a factor of 10. However, this lower river water flux was estimated for the Archean and is therefore likely an underestimate of the Proterozoic river flux.
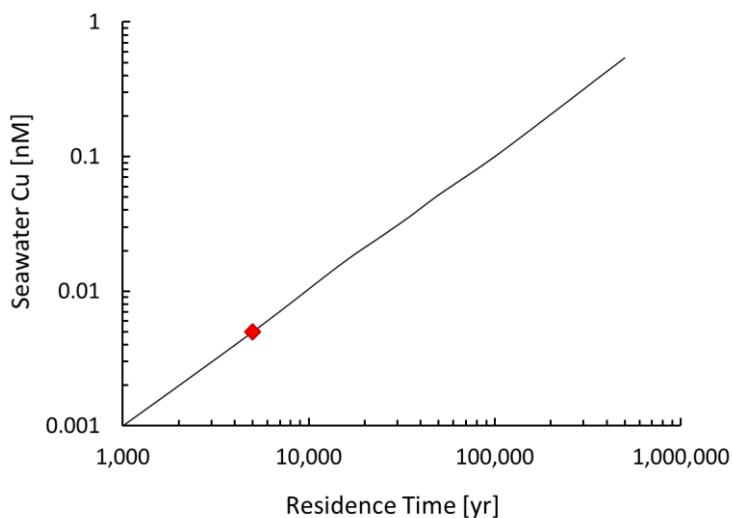
Figure S-7 Effect of increasing the total Cu residence time in the Archean ocean in a scenario with a high marine ligand (Ls) concentration of 1mM (Scenario 4 in Figure 1e in the main text). Unless ocean temperature was higher than today (Figure 1f in the main text), a longer residence time may be an alternative mechanism for maintaining nM levels of Cu_T in Archean seawater.

Supplementary Tables

Table S-1 Input data for the thermodynamic model. The hydrothermal fluid represents the Rainbow vent field in the Mid-Atlantic Ridge. Seawater constraints are described in the Methods. Note that the software requires that the two reacting fluids contain all constituents. Therefore, L_h and L_s had to be added also the seawater and the hydrothermal fluid, respectively, but their concentrations were set to extremely low values (10^{-20}), which are essentially zero for practical purposes.

Hydrothermal fluid			Modern seawater			Proterozoic seawater			Archean seawater		
Ba^{2+}	67	uM	Ba^{2+}	$9.21 \cdot 10^{-8}$	M	Ba^{2+}	$9.21 \cdot 10^{-8}$	M	Ba^{2+}	$9.21 \cdot 10^{-8}$	M
Ca^{2+}	67	mM	Ca^{2+}	$1.07 \cdot 10^{-2}$	M	Ca^{2+}	$1.07 \cdot 10^{-2}$	M	Ca^{2+}	$1.07 \cdot 10^{-2}$	M
Cl^-	750	mM	Cl^-	$5.91 \cdot 10^{-1}$	M	Cl^-	$5.91 \cdot 10^{-1}$	M	Cl^-	$5.91 \cdot 10^{-1}$	M
Cu^+	140	uM	Cu^+	$7.26 \cdot 10^{-9}$	nM	Cu^+	$7.26 \cdot 10^{-9}$	nM	Cu^+	$7.26 \cdot 10^{-9}$	nM
Fe^{2+}	24000	uM	Fe^{2+}	$1 \cdot 10^{-9}$	M	Fe^{2+}	100	uM	Fe^{2+}	100	uM
K^+	20	mM	K^+	$1.05 \cdot 10^{-2}$	M	K^+	$1.05 \cdot 10^{-2}$	M	K^+	$1.05 \cdot 10^{-2}$	M
L_h^-	10	uM	L_h^-	$1 \cdot 10^{-20}$	nM	L_h^-	$1 \cdot 10^{-20}$	nM	L_h^-	$1 \cdot 10^{-20}$	nM
L_s^-	$1 \cdot 10^{-20}$	nM	L_s^-	10	nM	L_s^-	10	nM	L_s^-	10	nM
Mg^{2+}	0.0001	nM	Mg^{2+}	$5.66 \cdot 10^{-2}$	M	Mg^{2+}	$5.66 \cdot 10^{-2}$	M	Mg^{2+}	$5.66 \cdot 10^{-2}$	M
Mn^{2+}	2250	uM	Mn^{2+}	$1 \cdot 10^{-9}$	M	Mn^{2+}	$1 \cdot 10^{-9}$	M	Mn^{2+}	$1 \cdot 10^{-9}$	M
Na^+	553	mM	Na^+	$5.06 \cdot 10^{-1}$	M	Na^+	$5.06 \cdot 10^{-1}$	M	Na^+	$5.06 \cdot 10^{-1}$	M
$SiO_{2(aq)}$	6.9	mM	$SiO_{2(aq)}$	$1.70 \cdot 10^{-4}$	M	$SiO_{2(aq)}$	$1.70 \cdot 10^{-4}$	M	$SiO_{2(aq)}$	$1.70 \cdot 10^{-4}$	M
Sr^{2+}	200	uM	Sr^{2+}	$1.33 \cdot 10^{-5}$	M	Sr^{2+}	$1.33 \cdot 10^{-5}$	M	Sr^{2+}	$1.33 \cdot 10^{-5}$	M
Zn^{2+}	160	uM	Zn^{2+}	$1.04 \cdot 10^{-8}$	M	Zn^{2+}	$1.04 \cdot 10^{-8}$	M	Zn^{2+}	$1.04 \cdot 10^{-8}$	M
$CH_{4(aq)}$	2.5	mM	HCO_3^-	$2.06 \cdot 10^{-3}$	M	HCO_3^-	$2.06 \cdot 10^{3}$	M	HCO_3^-	$2.06 \cdot 10^{-3}$	M
H_2S	1	mM	SO_4^{2-}	28	mM	SO_4^{2-}	$3 \cdot 10^{-3}$	M	SO_4^{2-}	20	uM
$H_{2(aq)}$	16	mM	$O_{2(aq)}$	349	uM	$O_{2(aq)}$	$3.49 \cdot 10^{-51}$	M	$H_{2(aq)}$	$7.90 \cdot 10^{-9}$	M
pH	4.8		pH	8.1		pH	7.5		pH	6.5	
T	300	°C	T	4	°C	T	4	°C	T	4	°C

Table S-2 Changing SO$_4^{2-}$ or Fe^{2+} in the Proterozoic ocean. These tests represent the scenario with 10 µM L$_h^+$ and 10 nM L$_s^+$. The second column shows the concentration of residual Cu in the fluid mixture after precipitation has ceased. Note the sudden decline in Cu levels when sulfate levels drop to 2 mM. 'Used' indicates the value that was used for the model in the main text.

Seawater SO$_4^{2-}$ [mM]	Final hydrothermal vent Cu [M]
2	$4.8 \cdot 10^{-11}$
3 (used)	$2.0 \cdot 10^{-9}$
4	$1.5 \cdot 10^{-9}$
5	$1.37 \cdot 10^{-9}$
10	$1.36 \cdot 10^{-9}$
Seawater Fe^{2+} [uM]	**Final hydrothermal vent Cu [M]**
100 (used)	$2.0 \cdot 10^{-9}$
1000	$1.83 \cdot 10^{-9}$

Table S-3 Changing SO$_4^{2-}$ or Fe^{2+} in the Archean ocean. These tests represent the scenario with 10 µM L$_h^+$ and 10 nM L$_s^+$. Residual Cu in the fluid more than doubles with increasing sulfate, but sulfate concentrations above 200 µM are probably unrealistic for the Archean ocean. 'Used' indicates the value that was used for the model in the main text.

Seawater SO$_4^{2-}$ [µM]	Final hydrothermal vent Cu [M]
2	$4.28 \cdot 10^{-12}$
20 (used)	$4.50 \cdot 10^{-12}$
200	$1.36 \cdot 10^{-11}$
2000	$1.63 \cdot 10^{-11}$
Seawater Fe^{2+} [uM]	**Final hydrothermal vent Cu [M]**
100 (used)	$4.50 \cdot 10^{-12}$
1000	$2.30 \cdot 10^{-12}$

Supplementary Information References

Al-Farawati, R., van den Berg, C.M. (1999) Metal–sulfide complexation in seawater. *Marine Chemistry* 63, 331-352.

Claire M.W., Catling D.C., Zahnle K.J. (2006) Biogeochemical modelling of the rise in atmospheric oxygen. *Geobiology* 4, 239-269.

Crowe, S.A., Paris, G., Katsev, S., Jones, C., Kim, S.T., Zerkle, A.L., Nomosatryo S., Fowle D., Adkins J.F., Sessions A.L., Farquhar J., Canfield D.E. (2014) Sulfate was a trace constituent of Archean seawater. *Science* 346, 735-739.

Emerson, S., Hedges, J. (2008) *Chemical oceanography and the marine carbon cycle.* Cambridge University Press, Cambridge, UK.

Halevy, I., Bachan, A. (2017) The geologic history of seawater pH. *Science* 355, 1069-1071.

Hao, J., Sverjensky, D.A., Hazen, R.M. (2017) Mobility of nutrients and trace metals during weathering in the late Archean. *Earth and Planetary Science Letters* 471, 148-159.

Holland, H.D. (1984) *The chemical evolution of the atmosphere and oceans,* Princeton University Press, Princeton, NJ.

Isson, T.T., Planavsky, N.J. (2018) Reverse weathering as a long-term stabilizer of marine pH and planetary climate. *Nature* 560, 471-475.

Jamieson, J.W., Wing, B.A., Farquhar, J., Hannington, M. (2013) Neoarchaean seawater sulphate concentrations from sulphur isotopes in massive sulphide ore. *Nature Geoscience* 6, 61-64.

Krissansen-Totton, J., Arney, G.N., Catling, D.C. (2018) Constraining the climate and ocean pH of the early Earth with a geological carbon cycle model. *Proceedings of the National Academy of Sciences* 115, 4105-4110.

Little, S.H., Vance, D., Walker-Brown, C., Landing, W.M. (2013) The oceanic mass balance of copper and zinc isotopes, investigated by analysis of their inputs, and outputs to ferromanganese oxide sediments. *Geochimica et Cosmochimica Acta* in press.

Luo, G., Ono, S., Huang, J., Algeo, T.J., Li, C., Zhou, L., Robinson, A., Lyons, T.W., Xie, S. (2014) Decline in oceanic sulfate levels during the early Mesoproterozoic. *Precambrian Research* 258, 36-47.

Lyons, T.W., Reinhard, C.T., Planavsky, N.J. (2014) The rise of oxygen in Earth's early ocean and atmosphere. *Nature* 506, 307-315.

Planavsky, N.J., McGoldrick, P., Scott, C.T., Li, C., Reinhard, C.T., Kelly, A.E., Chu, X., Bekker, A., Love, G.D., Lyons, T.W. (2011) Widespread iron-rich conditions in the mid-Proterozoic ocean. *Nature* 477, 448-451.

Raiswell, R. (2006) An evaluation ofdiagenetic recycling as a source of iron for banded iron formations. In: Kesler, S.E., Ohmoto, H. (Eds.) *Evolution of Early Earth's Atmosphere, Hydrosphere, and Biosphere: Constraints from Ore Deposits.* Geological Society of America Memoir, Boulder, Colorado, 223-238.

Reinhard, C.T., Planavsky, N.J., Robbins, L.J., Partin, C.A., Gill, B.C., Lalonde, S.V., Bekker, A., Konhauser, K.O., Lyons, T.W. (2013) Proterozoic ocean redox and biogeochemical stasis. *Proceedings of the National Academy of Sciences* 110, 5357-5362.

Sander, S.G., Koschinsky, A. (2011) Metal flux from hydrothermal vents increased by organic complexation. *Nature Geoscience* 4, 145-150.

Stüeken, E.E., Catling, D.C., Buick, R. (2012) Contributions to late Archaean sulphur cycling by life on land. *Nature Geoscience* 5, 722-725.

Tosca, N.J., Guggenheim, S., Pufahl, P.K. (2016) An authigenic origin for Precambrian greenalite: Implications for iron formation and the chemistry of ancient seawater. *GSA Bulletin* 128, 511-530.